Highlights

Correlation-based Feature Selection for Resilience Analysis of MVDC Shipboard Power System

Tazim Ridwan Billah Kushal,Mahesh S. Illindala

- All-electric ships can be made more resilient by appropriate design choices
- Feature selection approach can quantify effect of factors on resilience
- Case studies show that the modification of certain parameters can affect system performance during extreme event
- Features and performance indicators should reflect the desired characteristics of a resilient shipboard power system

Correlation-based Feature Selection for Resilience Analysis of MVDC Shipboard Power System

Tazim Ridwan Billah Kushal*, Mahesh S. Illindala

Department of Electrical and Computer Engineering, The Ohio State University, Columbus, OH 43210, USA

ARTICLE INFO

Keywords:
Contingency analysis
DC power system
Graph theory
Power system resilience
Shipboard power system

ABSTRACT

The future all-electric ship (AES) requires a resilient shipboard power system (SPS) that can withstand extreme events without substantial damage and maintaining critical capabilities. For superior capability to sustain disruptions, numerical measures of resilience provide assistance to engineers in making planning and operational decisions. This paper presents a novel method for analyzing the resilience characteristics of an SPS using correlation-based feature selection (CFS) to identify the system attributes that are the best predictors of performance during contingencies. Such attributes are typically chosen in the design stage and are not subject to modification during operation. The selected features are adjusted and their ramifications on the SPS performance are evaluated under the same contingencies. Results show quantitatively how a change of relevant attributes can improve or degrade the system performance in terms of unserved load and minimum recovery time.

1. Introduction

1.1. Background and Motivation

Electric power system is a critical piece of infrastructure in the next-generation ships, which are undergoing extensive research and development over the years. Recent advancements in the shipboard power system (SPS) include commissioning of an all-electric ship (AES) that uses electric propulsion system with advantages such as efficient fuel consumption, intelligent power management, and frequency decoupling brought about by solid-state power conversion devices [1, 2]. Due to several drawbacks of the conventional ac systems such as power quality issues, bulky transformers, and speed limitations of the generator prime movers, there is a growing interest in the development of medium-voltage dc (MVDC) solution for AES [1–3]. MVDC systems employ smaller size transformers as they use high-frequency power converters [1]. Electrification of ships enables easier integration of energy storage system (ESS) for better load management, fuel economy, and reduction of environmental impact by minimizing greenhouse gas emissions [2, 4, 5]. Moreover, ESS devices can be utilized as backup sources and energy accumulators for supplying pulse loads [2]. An MVDC SPS also simplifies the parallel operation of power sources since voltage phase and frequency matching is not necessary in dc systems [3].

Resilience may be defined as the ability of a system to withstand and recover from high-impact low-probability disruptive events [6, 7]. The concept of resilience exists in many disciplines, but for measurability it must be defined for a specific system [7]. A quantitative assessment of resilience is necessary to identify the relevant criteria, evaluate SPS performance, and design changes to make the system more resilient [8]. It is important to note that resilience is distinct from reliability since the two measures have different priorities. Reliability is measured using metrics such as the System Average Interruption Duration Index (SAIDI) and the System Average Interruption Frequency Index (SAIFI) [9], which assess the average SPS performance over an extended period. Since high-impact low-probability events such as natural disasters and major accidents are severely disruptive but rare, they have a minimal impact on reliability metrics and are therefore unsuitable for assessing the resilience. A reliable system is not necessarily resilient, so the development of additional metrics is needed in planning to minimize the performance degradation during extreme events [6]. This is critical for SPS because the ships often operate far away from land with no access to the larger terrestrial grid during emergencies.

1.2. Literature review

Various methods of analyzing and quantifying resilience exist in literature. Shinozuka et al. proposed the concept of resilience triangle based on the difference between pre-disturbance normal state and post-disturbance degraded state, and the speed of recovery [10]. To include additional information such as speed of degradation, duration of reduced performance state, and type of degradation, Panteli et al. developed metrics using a resilience trapezoid [11]. A computationally efficient analytical method for assessing the performance of microgrids against windstorms is presented in [12]. In [13], Francis and Bekera used a resilience analysis framework considering system-specific goals and vulnerabilities to develop a corresponding numerical measure based on recovery speed and performance during various post-disruption states. A dynamic Bayesian network was used to quantify resilience as a function of system availability [14]. Power distribution system resilience was evaluated by percolation theory and analytic hierarchy process (AHP) was employed to identify the most influential factors [15]. The restored network availability of a power distribu-

This work was supported in part by the U.S. Office of Naval Research under Grant N00014-16-1-2753.

*Corresponding author

kushal.1@osu.edu (T.R.B. Kushal); millindala@ieee.org (M.S. Illindala)

ORCID(s): 0000-0003-4626-8793 (T.R.B. Kushal)

https://dx.doi.org/10.1016/j.ijepes.2019.105742

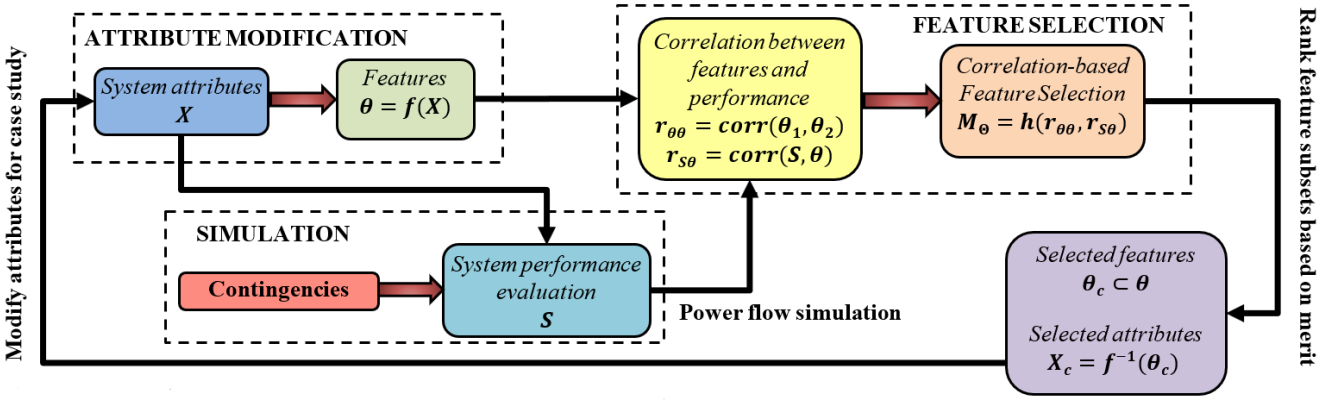

Figure 1: Proposed conceptual framework for resilience analysis using correlation-based feature selection.

tion system was used as the measure of resilience in a graph-theoretic formulation of the feeder restoration problem [16]. In [17], resilience is defined as a probability density function of network reliability when external factors cause component failure. Metrics based on spectral graph theory have been proposed for vulnerability assessment of power grids [18]. Recent research has also investigated the application of metrics inspired by natural ecosystems to quantification of power system resilience [19].

Resilience of SPS is critical due to its isolation and has been studied by a number of authors [20–23]. Network topologies for SPS were evaluated based on the critical order of contingency and average load shed per attack in [20]. Resilience control of a dc SPS was formulated as a two-stage optimization problem to maximize the survivability and critical load supply functionality [21]. In [22], the minimum number of sensors required to reconstruct lost data in a SPS following disruption was used as a measure of resilience. Song et al. proposed a resilience metric based on the reduction of large-scale ship automation system into component subsystems and implemented a control strategy in the ship's cooling water supply system [23]. In [24], a graph-theoretic power line expansion strategy was proposed to increase the SPS resilience.

1.3. Contribution

In the literature reviewed here, the approaches to quantify resilience have used different types of metrics, each with inherent limitations. Time-varying system performance [11, 12] has limited applicability for design and planning decisions because it relies on prediction of uncertain variables such as degradation rates and repair times. While service availability [14, 16] is a useful high-level indicator, it must be related to lower-level variables (such as network structure and component status) in order to be applicable for resilience-oriented design. This problem can be alleviated by using component failure as a measure [17, 22], although that does not consider the specific topology of the system. Graph theory based topological metrics [15, 18, 24] should be directly linked with performance indicators (eg. unserved electrical load) in order to be meaningful in resilience analysis. To overcome these limitations, some authors have considered multiple resilience criteria in their analyses. A mixture of topological and availability-based indicators are considered separately in [23] as a resilience vector, although they are not compared to each other. The authors of [15] used a multiple criteria decision analysis (MCDA) method to evaluate the relative importance of various topological resilience metrics. However, the weights assigned to the metrics in the MCDA process have been chosen subjectively and therefore reflect a qualitative decision process. An objective and quantitative basis for comparing different metric types is a critical step towards building a data-driven resilience analysis framework. This paper develops such a numerical comparison method based on correlation-based feature selection (CFS), which quantifies the predictive ability of feature subsets and ranks them accordingly [25].

CFS-based decision analysis offers numerous benefits to the design of SPS. Integration of intelligent control strategies for the growing number of power electronic devices has introduced new challenges for MVDC ship design [26]. The increasing complexity of SPS requires system-level approaches [27]. Recent works focused on the design of protection and control strategies [28–32], exploring the application of distributed energy storage [28, 29], fast protective devices [31], and advanced power electronics [27] to overcome the challenges to future AES. Design choices, such as the parameter selection in [30], are often motivated by dynamic stability. Resilience can be integrated into design considerations by, for instance, deciding the size and location of generators and energy storage across different zones on MVDC ships based on performance during extreme events. The proposed method could facilitate that integration by providing recommendations based on performance data and taking advantage of multiple metrics. It can be customized to any system where performance data is available.

1.4. Paper organization

The proposed resilience analysis of the SPS is presented in the following sections. A correlation-based method of

evaluating system features is introduced in Section 2. Section 3 defines the features and performance indicators used in the resilience analysis. Section 4 describes an MVDC PF model of the SPS that is used to evaluate the system performance under contingencies. Section 5 describes the results of applying the CFS methods to the aforementioned features and performance indicators and performs case studies based on the results. The conclusion of the paper is presented in Section 6.

2. Framework for resilience analysis using correlation-based feature selection

Fig. 1 illustrates the proposed conceptual framework for resilience analysis. Initially, the system attributes are defined and evaluated for specific measurable features of the SPS. Such attributes are fixed at the planning stage and not subject to changes during operation. Based on the same attributes, the performance of SPS is assessed by quantitative indicators. Next, the relationship between predefined features and performance indicators is quantified by calculating the correlation coefficients. These coefficients are fed into the CFS algorithm, which assigns merit scores to subsets of features based on predictive ability and redundancy. Since the dataset is generated by repeating the simulations for many contingency scenarios, the results from analysis are expected to give insights into the impacts of chosen attributes on resilience characteristics of the power system.

Correlation is a measure of the statistical dependence between two variables, and it can indicate a predictive relationship of practical value. Considering a set of bivariate data $(X, Y)_n$ for $n = 1, 2, 3, ..., m$, it is possible to predict the dependent variable Y according to its relationship with the independent variable X if there is a correlation between the two variables. Similar principles could be applied to multivariate data by extending the definition to include multiple independent variables [33]. For the SPS studied in this paper, it is of particular interest to determine the effect of certain parameters on the system resilience. Therefore, the system features are treated as independent variables and the performance indicators as dependent variables.

$$p(Y = y|X = x) \neq p(Y = y) \tag{1}$$

A feature X is said to be relevant to an output Y if and only if there are values x and y satisfying (1) [34]. Here, $p(Y = y)$ is the probability that an observation y of variable Y is made, and $p(Y = y|X = x)$ is the conditional probability of y given that observation x of variable X has been made. The essence of (1) is X and Y are not statistically independent and are therefore correlated. The prerequisite for this definition is $p(X = x) > 0$ since the relevant values of X must exist. The relevance of feature X to output Y depends on the degree of correlation, quantified by correlation coefficients. Pearson correlation coefficient is the most commonly used coefficient that can be calculated as $r_{X,Y} = cov(X, Y)/\sigma_X\sigma_Y$, where $cov(X, Y)$ is the covariance of X and Y, and σ_X and σ_Y are the variances of X and Y, respectively. It has a value between $+1$ and -1, with the sign indicating whether Y increases or decreases as X increases, and the magnitude is a numerical measure of the correlation. A value of 0 implies no correlation between the variables.

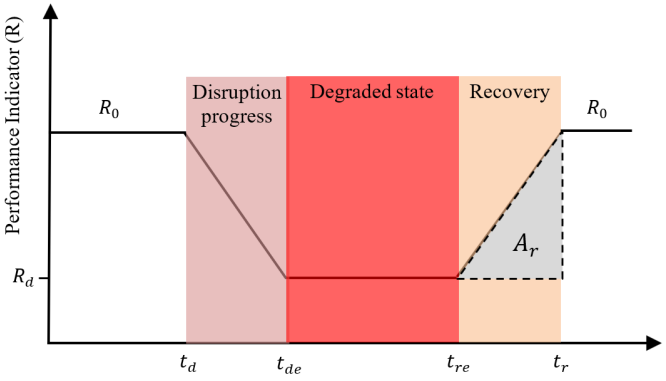

Figure 2: The resilience trapezoid, showing the different stages in the system after a disruptive extreme event.

Feature selection is an important step in the analysis of multivariate data due its ability to provide a greater understanding of the data-generating process by selecting the optimal feature set based on predictive ability [35]. CFS is a method of evaluating subsets of features using the principle that a good feature subset has characteristics highly predictive of the output but not of each other [25]. The absolute value of correlation coefficient is used as a measure of predictive ability. A feature subset Θ is evaluated by calculating its merit M_Θ using (2).

$$M_\Theta = \frac{k\overline{r_{S\theta}}}{\sqrt{k + k(k-1)\overline{r_{\theta\theta}}}} \tag{2}$$

The number of features in Θ is k, i.e., $k = |\Theta|$. Coefficient $\overline{r_{\theta\theta}}$ is the mean correlation between the features in Θ, and $\overline{r_{S\theta}}$ is the mean correlation between the features and unserved load S that indicates resilience. The numerator in (2) indicates the utility of a feature set in predicting the output, whereas the denominator gives a measure of the redundancy between the features of the set. A set containing redundant features has a high $\overline{r_{\theta\theta}}$, since the features are highly correlated with each other, and therefore they have a low merit score. Therefore, those features that are highly predictive of the output but statistically dependent on other features are discriminated against. The CFS algorithm calculates the merit for all subsets and ranks them accordingly. Generally, the subset with the highest merit score is used to select the most suitable attributes for a learning algorithm resulting in improved performance. In this paper, CFS is applied to quantify the relative significance of certain features in relation to system resilience, rather than to build a model for predicting the characteristics.

Nomenclature

P_i^g	active power output of generator at node i
x_i	commitment status of generator at node i
P_{ij}^L	active power flow from node i to j
D_i	active power demand at node i
S_i	unserved load at node i
V_i	voltage at node i
$\overline{V_i}, \underline{V_i}$	upper and lower bounds on voltage node i
$\overline{P_i^g}, \underline{P_i^g}$	maximum and minimum generation at node i
$\overline{P_{ij}^L}$	power flow capacity of line between nodes i and j
y_{ij}	operational status of line between nodes i and j
G_{ij}	conductance between nodes i and j
$RU_{i,max}$	ramp up limit of generator at node i
$RD_{i,max}$	ramp down limit of generator at node i

3. Resilience assessment methodology

3.1. Performance indicators

In general, a power system can be modeled as a simple undirected graph $\mathcal{G} = (\mathcal{V}, \mathcal{E})$ with $\mathcal{V} = \{1, 2, ..., n\}$ as the set of nodes and $\mathcal{E}$ as the set of edges, such that an edge from node i to j is denoted by an unordered pair $(i, j) \in \mathcal{E}$, which means that the two nodes are electrically connected. The set of neighbors of node i is denoted by $N_i = \{j \in \mathcal{V} | (j, i) \in \mathcal{E}\}$ and the cardinality of N_i is defined as its degree $deg(i) = |N_i|$ that is the number of edges where node i participates. Define two $n \times n$ matrices, adjacency matrix $\mathbf{A}$ and degree matrix $\mathbf{D}$, with elements as shown in (3)–(4). It is evident that $\mathbf{A}$ is a symmetrical matrix with all diagonal elements equal to zero and $\mathbf{D}$ is a diagonal matrix where all off-diagonal elements are zero.

$$a_{ij} = a_{ji} = \begin{cases} 1 & : (i, j) \in \mathcal{E} \\ 0 & : otherwise \end{cases} \quad \forall i, j \in \mathcal{V} \tag{3}$$

$$d_{ij} = \begin{cases} deg(i) & : i = j \\ 0 & : otherwise \end{cases} \quad \forall i, j \in \mathcal{V} \tag{4}$$

Simulation of the PF model provides numerical data from where both features and performance indicators can be extracted. However, since the resilience also measures the ability of a system to recover from a degraded state, its time-varying aspect must also be taken into account.

$$R = \sum_{i \in \mathcal{V}} \frac{D_i - S_i}{D_i} \tag{5}$$

$$A_r = \frac{(R_0 - R_d)(t_r - t_{re})}{2} \tag{6}$$

Fig. 2 shows the time-dependent performance of a power system during an extreme event as a resilience trapezoid [6, 11]. The first system performance indicator is the fraction of loads supplied R, described by (5). There are five distinct phases of system operation during the event. During the pre-disruption state $R = R_0$, and in the baseline normal operation scenario $R_0 = 1$, all loads are supplied. Moreover, in some cases shown later in the results, $R_0 < 1$; since certain system attributes are reduced to observe the effects on resilience. A disruptive event occurs at time t_d and the system performance degrades until time t_{de} when a new equilibrium is reached with $R = R_d$. This state lasts until restorative actions are undertaken and the system begins to recover. The restoration starts at timet_{re} and continues until the system returns to its normal operating state with $R = R_0$ at time t_r. Since the resilience of a system also includes its ability to recover from a degraded state, an additional resilience indicator is defined as the inverse of area A_r, given in (6) and shown in Fig. 2. If the system performance falls lower during the degraded state or it recovers more slowly, the area A_r increases implying the system is in a less resilient state. Therefore, the inverse of A_r, denoted by A_r^{-1}, is adopted as a measure of resilience. A higher value for these indicators corresponds to a more resilient system.

3.2. Feature definitions

Dynamic variables such as voltage and current vary over time during operation. On the other hand, fundamental attributes such as the system topology and available generation capacity typically remain unchanged during normal operation and change only in response to disruptive events. For the purposes of this study, we define a system *attribute* as a basic parameter of the SPS (such as generation limit, line flow capacity, and ramping limit) and a *feature* as a separate quantity calculated using the attributes. A feature may be equal to a single attribute or a composite of several attributes combined mathematically to indicate resilience.

1) Algebraic Connectivity: Spectral graph theory, which studies graphs quantitatively using associated matrices, has yielded several valuable insights on applying numerical measures to qualitative criteria [36]. Here, a resilience indicator is defined using ideas from spectral graph theory. The Laplacian matrix $\mathbf{L}$ is defined as $\mathbf{L} = \mathbf{D} - \mathbf{A}$, so that each off-diagonal element is $l_{ij} = l_{ji} = -a_{ij}$ and each diagonal element is $l_{ii} = deg(i)$. The second smallest eigenvalue of $\mathbf{L}$ is denoted by λ_2 and called the algebraic connectivity of a graph $\mathcal{G}$. It can be shown that $\lambda_2 = 0$ if and only if $\mathcal{G}$ is not connected, i.e., at least one node in $\mathcal{G}$ has no incident edges and is therefore isolated from the rest of the graph, and well-connected graphs have higher values of λ_2 [37]. For a power system, a well-connected graph indicates a better capability to serve the loads since more paths are available. Therefore, the algebraic connectivity is adopted as a resilience indicator, as in [18, 23].

2) Maximum Power Flow: Power system operation requires dispatching available generators to supply the existing demand in a timely and efficient manner, which may

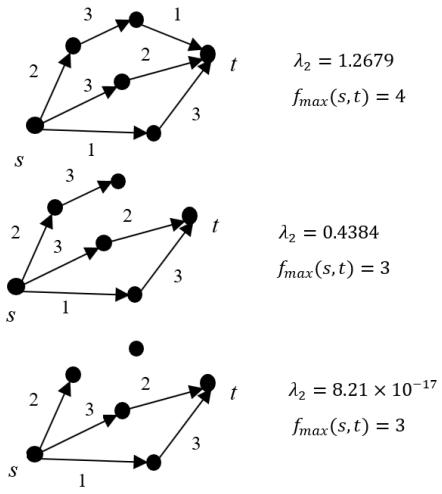

Figure 3: Graphical model of a sample subnetwork showing edge capacities and the effect of edge removal on λ_2 and f_{max}

be difficult during contingencies when network constraints are more restrictive. The problem of supplying power to a few nodes from other nodes can be formulated as a maximum flow problem in graph theory [38], described by (7)–(9). Since flow is directional, for this problem it is necessary to consider the graphical model of the SPS as a directed graph. Thus, (i, j) here represents an ordered pair of nodes, $\mathcal{E}^+$ is the set of directed edges and $f(i, j)$ is the flow from i to j. There is also a distinction between the neighbors of each node i such that the neighbor set N_i is partitioned into out-neighbors that receive flow from i and in-neighbors that send flow to i. The out-neighbor and in-neighbor sets are denoted by $N_i^- = \{j \in \mathcal{V} | (i, j) \in \mathcal{E}^+\}$ and $N_i^+ = \{j \in \mathcal{V} | (j, i) \in \mathcal{E}^+\}$, respectively.

$$\max_f f(s,t) \tag{7}$$

$$\sum_{j \in N_i^-} f(i,j) - \sum_{j \in N_i^+} f(j,i) = \begin{cases} |f(s,t)| & : i = s \\ -|f(s,t)| & : i = t \\ 0 & : otherwise \end{cases} \tag{8}$$

$$f(i,j) \leq c(i,j) \;\; (i,j) \in \mathcal{E}^+ \tag{9}$$

The objective of the maximum flow problem is to maximize the network flow $f(s, t)$ from a source s to a sink t without violating the constraints (8) and (9). The conservation equation (8) states that the net flow out of a node must equal the net flow into the node, except for source and sink nodes, where the net flow is equal to the desired maximum flow. Flow capacity limits are enforced by (9), where $c(i, j)$ is the capacity function of the edges (i, j). With SPS, $c(i, j) = c(j, i) = \overline{P_{ij}^L}$, the final value of the objective function is denoted by $f_{max}(\omega)$ and the maximum flow problem is solved by selecting a generator as the source and a load center as the sink. This is repeated for each generator-load pair. In Fig. 3, the effect of removing edges from a graph is shown by calculating maximum flow and algebraic connectivity for some test cases of a sample subnetwork.

3) Capacity-to-Load Ratio: If both feeders supplying a zonal load center are non-functioning, all the loads in that zone are disconnected from the bus. However, it is possible to supply the loads with at least one functioning feeder, without violating network constraints, if the line capacities are designed to be significantly higher than the demand during peak hours. Certain subsystems such as propulsion and heat, ventilation, and air conditioning (HVAC), can be considered critical loads and would be prioritized over other components by allocating higher capacity to the lines supplying them. Generally, a higher line capacity and lower magnitude of load means greater ease of supply, which enhances the resilience of SPS. Therefore, the capacity-to-load ratio (CLR) is defined as an indicator in (10).

$$CLR(\omega) = \sum_{d \in \mathcal{L}} \frac{\sum_{i \in \mathcal{V}} y_{id,\omega} \overline{P_{id}^L}}{D_d \sum_{i \in \mathcal{V}} y_{id,\omega}} \tag{10}$$

CLR is calculated as the sum of ratios of total maximum power flow capacity of connected lines to total connected loads for each load center. The subset of nodes associated with zonal load centers is denoted by $\mathcal{L}$.

4) Generation Capacity: Following a contingency, the amount of generation capacity (GC) available indicates the ability to supply loads. It is therefore an important factor that determines resilience. GC is calculated as the sum of the maximum output power of all connected generators for each scenario in (11). For the contingencies, it is assumed that the generators can operate at full capacity.

$$GC(\omega) = \sum_{i,j \in \mathcal{V}} y_{ij,\omega} \overline{P_i^g} \tag{11}$$

$$T_{dp}(\omega) = \begin{cases} \max\left(\frac{P_{i,\omega_d}^g - P_{i,\omega_0}^g}{RU_{i,max}}\right) & : P_{i,\omega}^g \geq P_{i,\omega_0}^g \\ \max\left(\frac{P_{i,\omega_0}^g - P_{i,\omega_d}^g}{RD_{i,max}}\right) & : P_{i,\omega}^g \leq P_{i,\omega_0}^g \end{cases} \tag{12}$$

5) Minimum Disruption Progression Time: The time interval $t_{de} - t_d$ in Fig. 2 is the disruption progression time, during which system performance is decreasing until it reaches a new stable operating point. The time taken to reach this new state is determined by several factors depending on the characteristics of power system. For the SPS studied here, the disruption progression time is constrained to a minimum by the ramping limits of generators. When the system transitions from pre-disruption normal state ω_0 to post-disruption degraded state ω_d, the generator setpoints must also change

to adapt to new operating conditions. The least time taken for the transition based on ramping limits is the minimum disruption progression time T_{dp} described in (12).

$$T_{ro}(\omega) = \begin{cases} \max\left(\frac{P^g_{i,\omega_d} - P^g_{i,\omega_0}}{RD_{i,max}}\right) & : P^g_{i,\omega} \geq P^g_{i,\omega_0} \\ \max\left(\frac{P^g_{i,\omega_0} - P^g_{i,\omega_d}}{RU_{i,max}}\right) & : P^g_{i,\omega} \leq P^g_{i,\omega_0} \end{cases} \quad (13)$$

6) Minimum Recovery Time: Recovery time for the SPS is given by $t_r - t_{re}$. It is the time required for the system to return to its normal state from post-disruption degraded state, which is the disruption progression in reverse. The minimum recovery time T_{ro} is defined in a manner similar to the minimum disruption progression time by (13). This is the same expression used for T_{dp} except that the order of scenarios is reversed since the system goes from ω_d to ω_0 during recovery.

It should be noted that both T_{ro} and T_{dp} are not the actual recovery and disruption progression times, but only the lower bounds. Actual times depend on several factors including availability and skill of repair crews as well as the nature of the disruptive event, which are beyond the scope of this paper. The analysis method proposed here considers only the system characteristics, irrespective of the nature of the disruptive event and restoration efforts.

4. Power flow modeling of MVDC shipboard power system

Fig. 5 illustrates the simplified schematic of SPS used in this study. The SPS employs a ring bus configuration, which offers a cost-effective and simple protection scheme that is flexible enough to remain operational when circuit breakers (CBs) are under repair [39]. Such a topology offers a major advantage for service restoration after an extreme event that damages a portion of the system. The loads in the SPS are grouped into six zonal load centers; each of them is supplied by two feeders from different sections of the bus. Four generators are connected at specific buses so that power delivery is still feasible when a section is offline. The operation of the SPS is modeled as a PF problem where the objective is to minimize the amount of unserved load without violating the constraints of the MVDC network. Since the purpose of the SPS is to supply the power demand, load shedding is the main indicator of the system health and is selected as the key numerical measure in the resilience analysis conducted here. The objective function of the optimization problem is given by (14) with variables $\Xi = \{x_i, P^g_i, P^L_{ij}, S_i, V_i \mid \forall i, j \in \mathcal{V}\}$. Appendix A contains the rest of equations in the model.

$$\min_{\Xi} \sum_{i \in \mathcal{V}} S_i \quad (14)$$

$$S_{tot}(\omega) = \sum_{i \in \mathcal{V}} S_i(\omega) \quad (15)$$

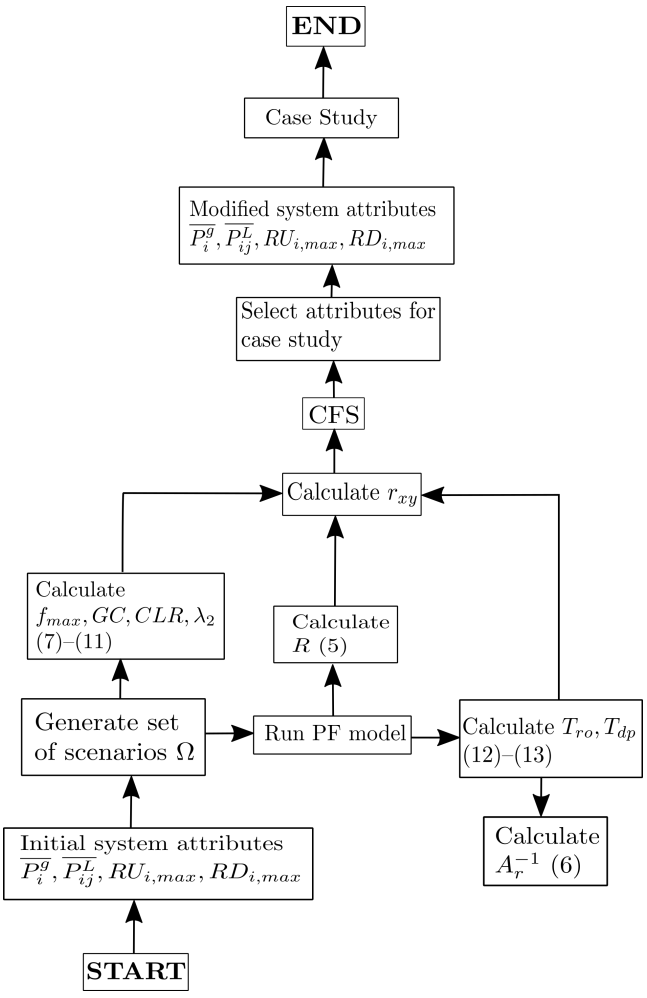

Figure 4: Resilience assessment and case study methodology.

To study the SPS under different contingencies, the PF model is solved for several scenarios where some lines are non-functional. The total unserved load for each scenario is evaluated in (15) as $S_{tot}(\omega)$ where ω denotes the scenario and Ω is the set of all scenarios considered. The set of contingencies captures not only the effect of power line disruptions but also generator failures, since disconnecting generators from the SPS has the same effect in terms of load shed. Disruption of lines can occur due to various reasons such as physical damage caused by accidents or deliberate attack, switchgear malfunction due to technical issues or malicious cyber attack. This study considers general scenarios where lines are disabled, so that the system resilience can be analyzed regardless of the cause of the failures.

5. Results and case studies

Fig. 4 illustrates the overall methodology for resilience assessment and numerical case study for SPS. Failure scenarios are generated combinatorially and the PF model is initialized with reference values of system attributes. Run-

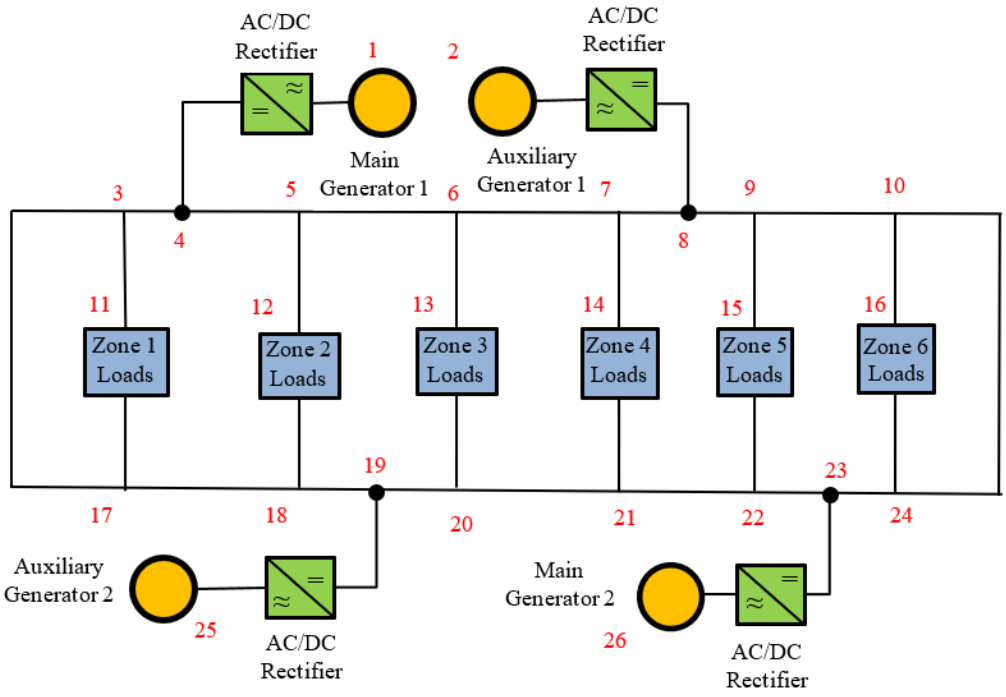

Figure 5: The ring bus configuration of the MVDC shipboard power system.

ning the PF model generates values for the features and performance indicators. Some features can be calculated without the PF model. Correlation coefficients are calculated for the results and CFS is used to rank feature subsets based on merit score. For the case study, selected system attributes are modified and PF is run again for all contingency scenarios.

Suppose the number of features is 6, the number of subsets containing at least one feature is found as $2^6 - 1 = 63$. Table 1 shows the 10 subsets with the highest merit scores in descending order. GC and T_{ro} jointly have the merit score of 0.7409 that is the highest among all the subsets. Adding T_{dp} reduces the score to 0.7128, showing that increasing the number of attributes does not improve the performance of the feature subset. In this particular case, the lower merit score can be attributed to the redundancy between T_{dp} and T_{ro}, since both depend on the generator ramping limits. Although most of the subsets in the list contain over one feature, this trend continues down the list and the addition of f_{max}, λ_2 and CLR result in significantly lower merit scores. Individual features are relatively poor predictors of resilience since only GC appears on the list with the ninth-highest merit score.

Solving the PF problem described in Section 4 for every scenario in Ω yields data about the operating state of the SPS during the contingencies, such as the generator setpoints, line power flows, and the total unserved load. Simulating all scenarios including various contingencies is computationally intensive, so the scenarios in Ω consider up to four simultaneous inactive power lines, which is enough to disable the entire SPS by cutting off all the loads from power supply. Higher-order contingencies having the same impact are unlikely to add new information about the features. The scenarios are generated combinatorially by disabling combinations of one, two, three, and four lines at a time. The test system contains 32 lines, resulting in 41,448 combinations of four or fewer inactive lines. By calculating the features described in Section 3 for each of these scenarios, the system resilience is studied.

Table 1 shows the results of CFS in the form of the top 10 feature subsets ranked by merit scores. Based on these rankings, the list of attributes to be modified for the case study are selected as shown in Fig. 4. Since the features are combinations of the attributes as shown in Section 3.2, modifying one attribute could affect multiple features. For example, changing generator ramping rates would affect both T_{ro} and T_{dp}, so considering them separately would be redundant. Cases are selected to ensure that the feature subsets reflect variation in a distinct set of attributes without overlap. Also, subsets including algebraic connectivity λ_2 are excluded from the cases because changing it would require changing the SPS topology while this study is limited to the configuration shown in Fig. 5.

To observe the effects of features on performance, the SPS power flow is simulated after changing some system attributes and their impact on the resilience indicators is measured. System performance is observed in four cases where

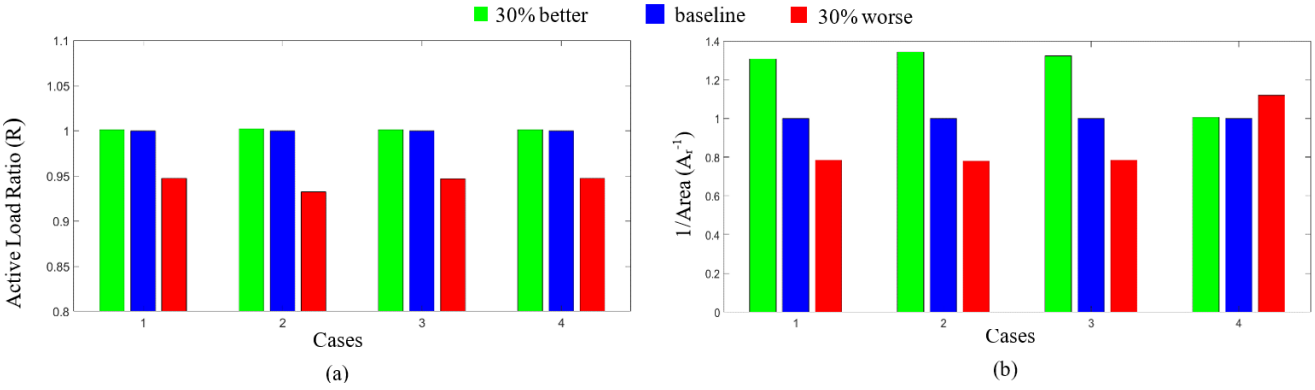

Figure 6: Performance indicators for different cases of changing attributes (a) fraction of loads supplied, and (b) A_r^{-1}.

Table 1
Feature subsets ranked by merit scores using CFS

Feature subset Θ	$\overline{r_{\theta\theta}}$	$\overline{r_{S\theta}}$	M_Θ
GC, T_{ro}	0.5291	0.6479	0.7409
GC, T_{ro}, T_{dp}	0.5351	0.5921	0.7128
GC, T_{dp}	0.3521	0.5665	0.6890
λ_2, GC, T_{ro}	0.5212	0.5670	0.6872
$\lambda_2, GC, T_{ro}, T_{dp}$	0.5260	0.5454	0.6793
f_{max}, GC, T_{ro}	0.5682	0.5722	0.6781
$f_{max}, GC, T_{ro}, T_{dp}$	0.5490	0.5493	0.6752
CLR, GC, T_{ro}, T_{dp}	0.3973	0.4832	0.6527
GC	-	0.6525	0.6525
$\lambda_2, f_{max}, GC, T_{ro}, T_{dp}$	0.5555	0.5205	0.6484

each case involves changes in different combinations of attributes. In each case, the attributes are varied over a range of $\pm$30% to have a positive or negative influence on resilience. The set of features tested in this case study consist of CLR, GC, T_{ro} and T_{dp}. The list of features for each case is given in Table 2 along with the results. CLR is improved by increasing the power flow capacities of the lines connecting load centers to the ring bus or reducing the load while increasing the capacities of all lines improves f_{max}. The load profile is not changed since it is not a design variable and depends on the operating state, but smaller loads would increase CLR and decrease load shedding. Increasing the maximum output of the generators improves GC. T_{ro} and T_{dp} can be jointly improved by increasing the ramping limits of the generators so they can reach the target setpoint faster. The results of the case study are demonstrated in Figs. 6 in terms of the performance indicators and Table 2 in terms of the percentage change in indicators.

The largest effect, both positive and negative, is seen in case 2, where the highest number of attributes is modified. Cases 1 and 3 cause similar percentage changes, showing that changing the flow capacities of distribution lines has little effect compared to modifying capacities of all power lines. Degrading the features noticeably influences the fraction of load supplied R as shown in Fig. 6. A 30% worsening

Table 2
Percentage change in resilience indicator for $\pm$30% change in attributes

Case	Features	R +30%	A_r^{-1} +30%	R −30%	A_r^{-1} −30%
1	GC, T_{ro}, T_{dp}	+0.13	+30.74	-5.27	-21.59
2	$f_{max}, GC, T_{ro}, T_{dp}$	+0.24	+34.40	-6.77	-22.04
3	CLR, GC, T_{ro}, T_{dp}	+0.13	+32.23	-5.31	-21.57
4	GC	+0.13	+0.57	-5.27	+12.02

of the features decreases R by about 5-7% compared to the baseline case. By contrast, a 30% improvement of the features has a much smaller effect on R, increasing it by not more than 0.24%. The effect of changing system attributes is much more significant when A_r^{-1} is used as the indicator. Cases 1-3 show more than 30% increase in resilience for attribute enhancement and over 20% decrease for attribute degradation. In case 4, where only GC is enhanced, A_r^{-1} increases by only 0.57% for the better case since the ramping limits are unchanged and the improvement in R is small. However, reducing the attributes positively influences A_r^{-1} for this case, although the effect on R is still negative and similar in magnitude to the other cases. An explanation for this anomalous result is that the reduced generation capacity in this case results in smaller changes in generator setpoints during transitions. Since the maximum ramping rates are unchanged, unlike cases 1-3, this leads to smaller T_{ro} and hence higher A_r^{-1}. This is supported by simulation results for reducing generation capacity by 30%, which show T_{ro} decreasing by 30.7% from baseline.

The results show an asymmetry in the positive and negative effects of attribute modification. Adding redundancy to the system in the form of higher-capacity generators and power lines yields slight benefits. However, reducing the redundancy has a larger negative impact on system performance. Therefore, CFS-based resilience analysis provides a numerical basis for adding redundancy to avoid catastrophic failures.

6. Conclusion

Resilience characteristics of an MVDC shipboard power system (SPS) have been studied by relating system attributes to performance indicators and evaluating the significance of the relationship using correlation-based feature selection. Features of interest are defined considering different aspects of the SPS and performance indicators provide information about the system operating state during contingencies and recovery options. Results are based on a power flow model where system attributes can be adjusted to observe the effect on performance. Combinations of attributes rather than individual attributes were found to truly illustrate the system resilience. The available generation capacity and minimum recovery time are particularly important factors in determining resilience, based on the relatively high correlation with unserved load. Results from case studies indicate that the system resilience is significantly impacted by variations in the selected attributes. In particular, a reduction in the parameters had severely degraded the system resilience.

The proposed CFS-based analysis is data-driven and can be applied to any system where performance data is available for a suitable range of possible contingencies. Numerical results will vary depending on the topology and scenario set used. The analysis will reveal factors that are most influential on system performance, which will vary from one power system to another. For example, topology is more significant in some configurations than others. Resilience of a radial power distribution system is expected to be strongly influenced by topology, other than the ring bus configuration of SPS, where loads have access to power supply through multiple lines. The proposed method could help engineers make system-specific decisions to the enhance resilience.

Simulation study of the resilience analysis method is limited to a subset of possible line failure contingencies, including cases with the worst possible consequences (total load shedding). For larger systems, the number of combinatorial possibilities increase rapidly and it may be necessary to select only the relevant scenarios in order for the problem to be computationally feasible. However, the analysis method would remain the same, since it can be applied to an arbitrary number of scenarios and features. The results have important implications for the design and planning of SPS using the MVDC solution. The attributes considered are assumed static and not subject to change. Interactions of these attributes with the performance of the SPS under high-impact events are complex and not readily apparent, therefore requiring a thorough numerical analysis. Planning decisions based on the framework proposed here can also include minor disruptive events, such as reduced fuel supply leading to decreased power generation and mechanical limitations in generators causing lower ramping rates. By providing insights into the relationships between parameters and performance, quantitative resilience analysis aids the power system planners in developing highly resilient systems.

Appendix A. MVDC power flow

The objective function (14) is subject to the following constraints:

$$P_i^g - \sum_{j \in N_i} P_{ij}^L = D_i - S_i \quad \forall i \in \mathcal{V}, \forall (i,j) \in \mathcal{E} \tag{A.1}$$

$$x_i \underline{P_i^g} \le P_i^g \le x_i \overline{P_i^g} \quad \forall i \in \mathcal{V} \tag{A.2}$$

$$\underline{V_i} \le V_i \le \overline{V_i} \quad \forall i \in \mathcal{V} \tag{A.3}$$

$$P_{ij}^L = y_{ij} G_{ij} V_i (V_i - V_j) \quad \forall i \in \mathcal{V}, \forall (i,j) \in \mathcal{E} \tag{A.4}$$

$$-y_{ij} \overline{P_{ij}^L} \le P_{ij}^L \le y_{ij} \overline{P_{ij}^L} \quad \forall (i,j) \in \mathcal{E} \tag{A.5}$$

The power balance equation (A.1) makes the sum of active power flowing into each node equal to zero. Power generation limits are enforced by (A.2), where x_i takes the value of 1 when the generator is online and 0 when it is offline. Node voltage V_i must remain within the upper bound $\overline{V_i}$ and lower bound $\underline{V_i}$, as shown in (A.3). Equation (A.4) describes the active power flow in the line between nodes i and j, where y_{ij} has a value of 1 when the line is operational and 0 when it is not. For the simulations in this paper, a certain set of lines is considered non-operational for each scenario, so y_{ij} is a parameter rather than a variable of the optimization problem. Line flow capacity $\overline{P_{ij}^L}$ is imposed in (A.5).

$$U_i = V_i - V_{ref} \tag{A.6}$$

$$\underline{V_i} - V_{ref} \le U_i \le \overline{V_i} - V_{ref} \tag{A.7}$$

$$P_{ij}^L = y_{ij} G_{ij} (U_i - U_j) \tag{A.8}$$

The non-linear expression in (A.4) can be linearized using the assumption that node voltages vary only slightly from the nominal voltage [40]. The linearization method has been previously used for MVDC SPS in [20], and is used in this paper. Equations (A.6)–(A.8) do this by defining the node voltages as deviations from a reference bus voltage V_{ref}, which can be calculated from a known bus voltage. If it is known that $V_i = 1.0$ p.u., then $V_{ref} = 0$ p.u., and (A.4) can be approximated by the linear expression in (A.8). The new voltage bounds in (A.7) are obtained from (A.3) using the same reference.

References

[1] Jin Z, Sulligoi G, Cuzner R, Meng L, Vasquez JC, Guerrero JM. Next-Generation Shipboard DC Power System: Introduction Smart Grid and dc Microgrid Technologies into Maritime Electrical Netowrks. IEEE Electrif Mag 2016;4:45–57. doi:10.1109/MELE.2016.2544203.

[2] Sudhoff S. Currents of Change. IEEE Power Energy Mag 2011;9:30–7. doi:10.1109/MPE.2011.941319.

[3] Doerry N. Naval Power Systems: Integrated power systems for the continuity of the electrical power supply. IEEE Electrif Mag 2015;3:12–21. doi:10.1109/MELE.2015.2413434.

[4] Kanellos FD. Optimal Power Management With GHG Emissions Limitation in All-Electric Ship Power Systems Comprising Energy Storage Systems. IEEE Trans Power Syst 2014;29:330–9. doi:10.1109/TPWRS.2013.2280064.

[5] Prousalidis JM, Tsekouras GJ, Kanellos F. New challenges emerged from the development of more efficient electric energy generation units. 2011 IEEE Electr. Sh. Technol. Symp., Alexandria, VA: IEEE; 2011, p. 374–81. doi:10.1109/ESTS.2011.5770901.

[6] Bie Z, Lin Y, Li G, Li F. Battling the Extreme: A Study on the Power System Resilience. Proc IEEE 2017;105:1253–66. doi:10.1109/JPROC.2017.2679040.

[7] Watson et al. J-P. Conceptual Framework for Developing Resilience Metrics for the Electricity, Oil, and Gas Sectors in the United States (September 2015) | Department of Energy. Albuquerque, NM: 2015.

[8] Committee on Increasing National Resilience to Hazards and Disasters. Disaster Resilience: A National Imperative. Washington, DC: 2012.

[9] Eto JH, LaCommare KH, Sohn MD, Caswell HC. Evaluating the Performance of the IEEE Standard 1366 Method for Identifying Major Event Days. IEEE Trans Power Syst 2017;32:1327–33. doi:10.1109/TPWRS.2016.2585978.

[10] Shinozuka M, Chang SE, Cheng T, Feng M, O'Rourke TD, Saadeghvaziri MA, et al. Resilience of Integrated Power and Water Systems. Seism Eval Retrofit Lifeline Syst 2003:65–86.

[11] Panteli M, Mancarella P, Trakas DN, Kyriakides E, Hatziargyriou ND. Metrics and Quantification of Operational and Infrastructure Resilience in Power Systems. IEEE Trans Power Syst 2017;32:4732–42. doi:10.1109/TPWRS.2017.2664141.

[12] Amirioun MH, Aminifar F, Lesani H, Shahidehpour M. Metrics and quantitative framework for assessing microgrid resilience against windstorms. Int J Electr Power Energy Syst 2019;104:716–23. doi:10.1016/j.ijepes.2018.07.025.

[13] Francis R, Bekera B. A metric and frameworks for resilience analysis of engineered and infrastructure systems. Reliab Eng Syst Saf 2014;121:90–103. doi:10.1016/J.RESS.2013.07.004.

[14] Cai B, Xie M, Liu Y, Liu Y, Feng Q. Availability-based engineering resilience metric and its corresponding evaluation methodology. Reliab Eng Syst Saf 2018;172:216–24. doi:10.1016/j.ress.2017.12.021.

[15] Chanda S, Srivastava AK. Defining and Enabling Resiliency of Electric Distribution Systems With Multiple Microgrids. IEEE Trans Smart Grid 2016;7:2859–68. doi:10.1109/TSG.2016.2561303.

[16] Dubey A, Poudel S. A robust approach to restoring critical loads in a resilient power distribution system. 2017 IEEE Power Energy Soc. Gen. Meet., Chicago, IL: IEEE; 2017, p. 1–5. doi:10.1109/PESGM.2017.8274597.

[17] Whitson JC, Ramirez-Marquez JE. Resiliency as a component importance measure in network reliability. Reliab Eng Syst Saf 2009;94:1685–93. doi:10.1016/J.RESS.2009.05.001.

[18] Rocchetta R, Patelli E. Assessment of power grid vulnerabilities accounting for stochastic loads and model imprecision. Int J Electr Power Energy Syst 2018;98:219–32. doi:10.1016/j.ijepes.2017.11.047.

[19] Panyam V, Huang H, Davis K, Layton A. Bio-inspired design for robust power grid networks. Appl Energy 2019. doi:10.1016/j.apenergy.2019.113349.

[20] Jothibasu S, Santoso S. New Electric Shipboard Topologies for High Resiliency. IEEE Trans Power Syst 2018;33:2975–83. doi:10.1109/TPWRS.2017.2756027.

[21] Li J, Liu F, Chen Y, Shao C, Wang G, Hou Y, et al. Resilience Control of DC Shipboard Power Systems. IEEE Trans Power Syst 2018;PP:1–1. doi:10.1109/TPWRS.2018.2844161.

[22] Dustegor D, Mezyani T El, McLaren PG. A sensor failure resilience metric for ship-board power system. 2011 IEEE Electr. Sh. Technol. Symp., Alexandria, VA: IEEE; 2011, p. 240–3. doi:10.1109/ESTS.2011.5770874.

[23] Song Z, Ren G, Mirabella L, Srivastava S. A resilience metric and its calculation for ship automation systems. 2016 Resil. Week, Chicago, IL: IEEE; 2016, p. 194–9. doi:10.1109/RWEEK.2016.7573332.

[24] Lai K, Illindala M. Graph Theory-based Shipboard Power System Expansion Strategy for Enhanced Resilience. IEEE Trans Ind Appl 2018;PP:1–1. doi:10.1109/TIA.2018.2860941.

[25] Hall MA, Holmes G. Benchmarking attribute selection techniques for discrete class data mining. IEEE Trans Knowl Data Eng 2003;15:1437–47. doi:10.1109/TKDE.2003.1245283.

[26] Zohrabi N, Shi J, Abdelwahed S. An overview of design specifications and requirements for the MVDC shipboard power system. Int J Electr Power Energy Syst 2019;104:680–93. doi:10.1016/j.ijepes.2018.07.050.

[27] Wang F, Zhang Z, Ericsen T, Raju R, Burgos R, Boroyevich D. Advances in Power Conversion and Drives for Shipboard Systems. Proc IEEE 2015;103:2285–311. doi:10.1109/JPROC.2015.2495331.

[28] Jin Z, Meng L, Guerrero JM, Han R. Hierarchical control design for a shipboard power system with DC distribution and energy storage aboard future more-electric ships. IEEE Trans Ind Informatics 2018;14:703–14. doi:10.1109/TII.2017.2772343.

[29] He L, Li Y, Shuai Z, Guerrero JM, Cao Y, Wen M, et al. A flexible power control strategy for hybrid AC/DC zones of shipboard power system with distributed energy storages. IEEE Trans Ind Informatics 2018;14:5496–508. doi:10.1109/TII.2018.2849201.

[30] Lin G, Li Y, Liu J, Li C. Resonance analysis and active damping strategy for shipboard DC zonal distribution network. Int J Electr Power Energy Syst 2019;105:612–21. doi:10.1016/j.ijepes.2018.08.038.

[31] Qi LL, Antoniazzi A, Raciti L, Leoni D. Design of Solid-State Circuit Breaker-Based Protection for DC Shipboard Power Systems. IEEE J. Emerg. Sel. Top. Power Electron., vol. 5, Institute of Electrical and Electronics Engineers Inc.; 2017, p. 260–8. doi:10.1109/JESTPE.2016.2633223.

[32] Babaei M, Jafari-Marandi R, Abdelwahed S, Kluss J. A novel approach for real-time implementation of MVDC shipboard power system reconfiguration. Int J Electr Power Energy Syst 2018;100:240–52. doi:10.1016/j.ijepes.2018.01.037.

[33] Croxton FE, Cowden DJ, Klein S. Applied General Statistics. Prentice-Hall, Inc.; 1967.

[34] Kohavi R, John GH. Wrappers for feature subset selection. Artif Intell 1997;97:273–324. doi:10.1016/s0004-3702(97)00043-x.

[35] Guyon I, Elisseeff A. An Introduction to Variable and Feature Selection. J Mach Learn Res 2003;3:1157–82.

[36] Spielman D. Spectral Graph Theory. Comb. Sci. Comput., CRC Press; 2012.

[37] Fiedler M. Algebraic connectivity of graphs. Czechoslov Math J 1973;23:298–305.

[38] Ford LR, Fulkerson DR. Flows in Networks. Princeton University Press; 2010.

[39] Anderson PM. Power System Protection. Wiley-IEEE Press; 1998.

[40] Iggland E, Wiget R, Chatzivasileiadis S, Anderson G. Multi-Area DC-OPF for HVAC and HVDC Grids. IEEE Trans Power Syst 2015;30:2450–9. doi:10.1109/TPWRS.2014.2365724.